X-ray transition radiation by high-energy electrons in a thin solid target placed in an external magnetic field

I. V. Demydenko* and S. V. Trofymenko

V.N. Karazin Kharkiv National University, Svobody, Square 4, 61022, Kharkiv, Ukraine and National Science Center, "Kharkiv Institute of Physics and Technology," Akademichna street 1, 61108, Kharkiv, Ukraine

A. P. Potylitsyn

Institute of Applied Problems of Physics, Hrachya Nersisyan Street 25, 0014, Yerevan, Armenia

G. Kube

Deutsches Elektronen-Synchrotron (DESY), Notkestraße 85, D-22607, Hamburg, Germany

A. V. Shchagin

National Science Center, "Kharkiv Institute of Physics and Technology," Akademichna street 1, 61108, Kharkiv, Ukraine and Deutsches Elektronen-Synchrotron (DESY), Notkestraße 85, D-22607, Hamburg, Germany

(Received 23 July 2025; accepted 4 December 2025; published 18 December 2025)

X-ray transition radiation emitted by high-energy electrons in a thin foil placed in a strong external magnetic field is considered. The modification of the radiation properties resulting from the bending of the particle's trajectory in the magnetic field is investigated. It is shown that, due to the interference between transition and synchrotron radiation, the total radiation spectrum can significantly differ from the simple sum of the conventional spectra of these two types of emission. Both constructive and destructive interference can occur in this case. The dependence of the magnitude of this interference on the electron energy and the acceptance angle of the radiation detector is analyzed.

DOI: 10.1103/dwpb-9dm7

I. INTRODUCTION

Transition radiation (TR) is emitted when a charged particle crosses the interface between two media with different dielectric permittivities. Generally, it has a broad spectrum involving THz, infrared, optical, ultraviolet, and—for ultrarelativistic particles—also x-ray frequency ranges. In the THz and optical ranges, this radiation plays an important role in accelerator physics, serving as an effective tool for diagnosing the parameters of charged particle beams [1–3]. X-ray TR is widely used for the detection of high-energy particles [4]. Moreover, for a fixed photon energy, x-ray TR can be emitted only by particles with a Lorentz factor γ exceeding some minimal threshold value, which allows applying this radiation for separating light and heavy particles. X-ray TR is also applied as a source of x-ray photons for various purposes [5–8]. Thus, investigating the properties of TR under various conditions is of great interest both from the fundamental point of view and for the development and improvement of technologies based on this radiation.

For the process of TR emission (as well as for other types of electromagnetic radiation), a considerable role is played by the parameter known as the formation length l_F [9]. It defines some effective region of space around the interface (l_F is usually defined separately on each side of the interface), which is responsible for the formation of the TR pulse and depends on the particle energy, radiation frequency, observation direction, and the properties of the medium where TR propagates. If the particle motion is somehow disturbed within this region (e.g., the particle changes its direction of motion or crosses other interfaces), the TR characteristics can be dramatically modified. It can be considered as a result of interference of a conventional TR for an "undisturbed" rectilinear particle motion and radiation emitted by the particle as a result of the disturbance. At high particle energies, the value of l_F can become

*Contact author: iliademydenko@gmail.com

macroscopically large, and such an effect may be unavoidable in a real experiment. This effect has been studied both theoretically and experimentally for different types of particle interaction within the distance l_F from the interface and for various TR frequencies. Particularly, this includes investigations of TR by "half-bare" electrons (this term was introduced in [10]), when the electron loses its conventional Coulomb field as a result of scattering [11] or passing through an upstream target [12–15] before impinging on the downstream target and generating TR in the millimeter and optical wavelength regions. In these works, both the effects of suppression and enhancement of the TR intensity from the downstream target, compared to the TR by an incident electron with the conventional Coulomb field, have been predicted or observed. The analogous effects of the formation length have also been investigated for the x-ray TR by high-energy electrons in multifoil radiators both earlier [16,17] and recently [18,19]. In such radiators, the role of the mentioned disturbance preceding the electron passage through the nth foil of the radiator is played by the preliminary passage of the particle through the $(n-1)$th foil.

The effects associated with a large size of the formation length and the half-bare state of the particle have been theoretically and experimentally investigated also for other processes taking place at high-energy particle interaction with media. Initially, they were studied for bremsstrahlung, which led to the discovery of the Landau-Pomeranchuk-Migdal [20–22], Ternovskii-Shul'ga-Fomin [23–25], and Ter-Mikaelyan [9,26] effects of suppression of bremsstrahlung by high-energy electrons in amorphous media. Further investigations concerned the processes of diffraction radiation [27], coherent x-ray emission in crystals [28,29], and ionization energy loss [30]. In [31], the formation region effects were discussed for the so-called edge radiation generated at the entrance of a particle into a magnetic field. In [32], the influence of a magnetic field on TR (in the radio frequency range) emitted by ultrarelativistic particles interacting with random density inhomogeneities in a turbulent plasma under astrophysical conditions was investigated. It was shown that the bending of the particle trajectory by the field can lead to suppression of the TR intensity.

In the present paper, we discuss a different statement of the problem about the influence of the external magnetic field on TR, which can be relevant for various laboratory experiments involving x-ray TR, as well as TR detectors. Specifically, we consider x-ray TR emitted by multi-GeV electrons in a thin target placed in a strong external magnetic field. It is noted that for realistic values of the magnetic field, even in the x-ray range of frequencies, the formation length l_F can be larger than the typical distance on which the electron deflects to an angle of about $1/\gamma$ under the impact of the magnetic field. In this case, the particle leaves the typical radiation cone of TR with the opening angle $\sim 1/\gamma$ within the formation length, which results in a modification of the radiation characteristics.[1] It can be considered as a result of interference between the TR and the synchrotron radiation (SR) emitted by the particle in the vicinity of the target. It is shown that such interference can be both destructive and constructive, resulting in a decrease or enhancement of the total radiation intensity compared to the sum of independent TR and SR. It should be noted that in [33], the influence of an external magnetic field on TR emitted at a particle's exit from a conducting target was investigated for much lower frequencies, where the radiation properties differ from those in the x-ray range. Namely, the consideration presented in [33] is valid up to infrared frequencies, where the target can be regarded as an ideal conductor. The main attention there was devoted to the study of azimuthal asymmetry in the TR angular distribution.

Placing the target in the external magnetic field is a nice way to remove the background radiation coming together with the incident electron beam. For instance, if the target is placed in the center of the deflecting magnet, the investigated radiation from the target (e.g., TR or bremsstrahlung) propagates in the direction between the background and the final direction of the electron beam. However, such a configuration requires taking into account the influence of the magnetic field on the TR characteristics, which are investigated in the present paper. In particular, in measurements of bremsstrahlung, this modified TR is itself a form of radiation that should be carefully subtracted from the total signal (this was precisely the challenge the authors encountered in the experiments at the DESY II test beam facility, which motivated the present investigation). The results obtained in the present paper are also of interest for a better understanding of the operation of particle detectors based on x-ray TR, when they are placed in an external magnetic field [34,35].

II. METHOD OF CALCULATION

Generally, in order to calculate the TR spectral-angular distribution, it is necessary to solve the Maxwell's equations with proper boundary conditions on the surfaces of the target. If the radiating particle moves along some curvilinear trajectory, such an approach can be cumbersome and application of simplified methods is relevant. An example of such a method has been introduced in [36,37] for investigating the influence of multiple scattering of the particle in the target on TR. Let us adjust it for the conditions we are presently interested in, which correspond to ultrarelativistic electrons and radiated photon energies exceeding several keV. The discussed method is based on the well-known expression for the spectral-angular

[1]As in the case of the Landau-Pomeranchuk-Migdal effect, where the particle leaves the typical cone of bremsstrahlung within the formation length, which results in the suppression of this radiation.

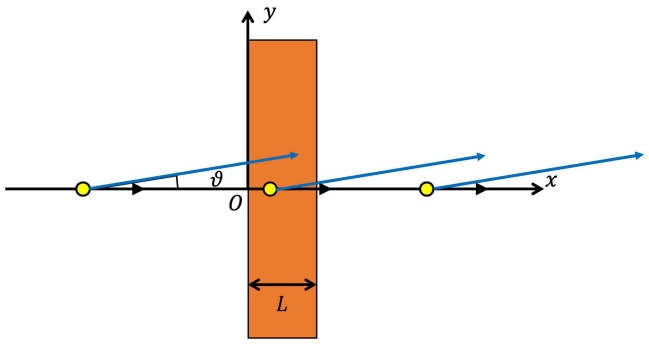

FIG. 1. Passage of a particle through a target in vacuum.

distribution of radiation by a charged particle moving in vacuum and with position $\mathbf{r}(t)$ and velocity $\mathbf{v}(t)$ [38]:

$$\frac{d^2I}{d\omega\, do} = \frac{e^2\omega^2}{4\pi^2c^3}\left|\int_{-\infty}^{\infty} dt\mathbf{n}\times\mathbf{v}(t)e^{i\omega(t-\mathbf{nr}(t)/c)}\right|^2, \quad (1)$$

where e is the charge of the particle, ω is the radiation frequency, and $\mathbf{n}$ is a unit vector along the observation direction. Expression (1) has the form of an integral over the waves emitted by the particle at each point of its trajectory, which can be formally considered as real electromagnetic waves. If such a wave penetrates through a layer of medium on its way to the detector (e.g., when the particle passes through a target), it acquires a different phase shift compared to propagation in a vacuum. This is due to the fact that inside the medium the wave vector is given by the expression $\mathbf{k} = \omega\mathbf{n}\sqrt{\varepsilon}/c$, where ε is the dielectric permittivity of the medium.

Let us consider the case where the particle moves rectilinearly along the x axis and normally passes through a plate of thickness L situated in vacuum in the region $x \in [0, L]$ (see Fig. 1). Consider the waves emitted by the particle in the region $x < 0$, which pass through the plate on their way to the detector. Due to the axial symmetry, one can just consider the waves propagating in the xy plane. A wave that traveled a distance $\Delta\mathbf{r}$ gets the phase shift:

$$\mathbf{k}\Delta\mathbf{r} = k_x\Delta x + k_y\Delta y. \quad (2)$$

For ultrarelativistic particles, the major part of radiation is emitted at small angles $\vartheta << 1$ with respect to the particle's velocity. In this case, one can estimate: $k_x \sim \omega/c$ and $k_y \sim \omega\vartheta/c$ (both in vacuum and in the medium since $\varepsilon \approx 1$ in the x-ray range). Taking into account that $\Delta y = \vartheta\Delta x$, we have $|k_y\Delta y| \sim |k_x\Delta x|\vartheta^2$.

In the x-ray frequency range, the target permittivity can be written as $\varepsilon = 1 - \omega_p^2/\omega^2 + i\mu c/\omega$, where ω_p is the plasma frequency of the target and $\mu(\omega)$ is the energy attenuation coefficient of the target, which we calculate on the basis of [39]. Since $\mu c/\omega$ and ω_p^2/ω^2 are small quantities,

$$\sqrt{\varepsilon} \approx 1 - \frac{\omega_p^2}{2\omega^2} + \frac{i\mu c}{2\omega}. \quad (3)$$

Therefore, to second order in ϑ, the first term in (2) makes the following contribution to the additional phase shift of the considered waves inside the target (i.e., in the region $0 < x < L$), compared to the corresponding phase shift in the absence of the target:

$$\Delta\phi_x = \frac{\omega L}{c}(\sqrt{\varepsilon} - 1) \approx -\frac{\omega_p^2 L}{2\omega c}(1 - \vartheta^2/2) + \frac{i\mu L}{2}(1 - \vartheta^2/2). \quad (4)$$

The typical values of the relevant parameters considered in this work are as follows: an aluminum target with thickness $L \leq 50$ μm, a radiation frequency[2] of $\omega \sim 15$ keV, and a detector acceptance angle smaller than several mrad. In this case, we have $\omega_p^2 L/(2\omega c) \sim 10$ and $\mu L \sim 0.1$, and it is possible to neglect the quadratic terms in (4). This also allows neglecting the contribution of the second term in (2) and presenting the resulting additional phase shift (due to the presence of the target) for the waves emitted in the region $x < 0$ as

$$\Delta\phi = -\frac{\omega_p^2 L}{2\omega c} + \frac{i\mu L}{2}. \quad (5)$$

The waves emitted inside the target acquire the same additional phase shift as (5), but with the substitution $L \to L - x = L - vt$. Generally, these waves have a different amplitude compared to those emitted in vacuum. It is associated with the additional factor $\sqrt{\varepsilon}$, which appears in front of the formula (1) when it is derived for a particle moving in a homogeneous medium with permittivity ε (together with the substitution $\omega\mathbf{n}/c \to \sqrt{\varepsilon}\omega\mathbf{n}/c$ in the exponent) [40]. However, since in the x-ray range ε is very close to 1, we will consider the amplitude of these waves to be the same as for the waves emitted in vacuum. For the same reason, we neglect the refraction of the waves on the surfaces of the target. Naturally, the waves emitted after the target do not acquire any additional phase shift.

In order to obtain the spectral-angular distribution of TR in the considered case, it is necessary to add the obtained phase shifts to the argument of the exponent in (1). As a result, neglecting the small terms $\mu c/\omega$ in the denominators, one gets the well-known expression [41,42] for the spectral-angular distribution of the number of TR photons ($d^2N/dod\omega = (\hbar\omega)^{-1}d^2I/dod\omega$):

[2]We assume that the Planck constant $\hbar = 1$ (it is written explicitly in some places for the sake of convenience), thus identifying frequencies and photon energies.

$$\frac{d^2N}{d\omega do} = \frac{\alpha}{\pi^2\omega}\vartheta^2\frac{\omega_p^4}{\omega^4}\frac{1+e^{-\mu L}-2e^{-\mu L/2}\cos(L/l_F)}{(\gamma^{-2}+\vartheta^2)^2(\gamma^{-2}+\vartheta^2+\omega_p^2/\omega^2)^2}, \tag{6}$$

where $\alpha \approx 1/137$ is the fine structure constant and

$$l_F = \frac{2c}{\omega(\gamma^{-2}+\vartheta^2+\omega_p^2/\omega^2)} \tag{7}$$

is the radiation formation length inside the target.

III. ANGLELIKE TRAJECTORY

To illustrate the influence of particle deflection within the formation length on TR, emitted as the particle passes through a target, and the arising interference effects, let us first consider a simplified and idealized case of particle motion along an anglelike trajectory. Let an electron traverse a target and immediately deflect to some angle χ at the exit of the target, as shown in Fig. 2.

Applying the method described in Sec. II, one obtains the following result for the radiation spectral-angular density in this case:

$$\frac{d^2N}{d\omega do} = \frac{\alpha}{\pi^2\omega}e^{-\mu_a d}[|J_y|^2+|J_z^2|], \tag{8}$$

where J_y and J_z are defined as follows:

$$J_y = \vartheta\sin\phi\left[\frac{e^{-\mu L/2}}{Q(0)}+\frac{e^{iL/l_F}-e^{-\mu L/2}}{\gamma^{-2}+\vartheta^2+\omega_p^2/\omega^2}-\frac{e^{iL/l_F}}{Q(\chi)}\right], \tag{9}$$

where $Q(\chi)=\gamma^{-2}+\vartheta^2+\chi^2-2\chi\vartheta\cos\phi$ and

$$J_z = \vartheta\cos\phi\left[\frac{e^{-\mu L/2}}{Q(0)}+\frac{e^{iL/l_F}-e^{-\mu L/2}}{\gamma^{-2}+\vartheta^2+\omega_p^2/\omega^2}\right] + \frac{(\chi-\vartheta\cos\phi)}{Q(\chi)}e^{iL/l_F}. \tag{10}$$

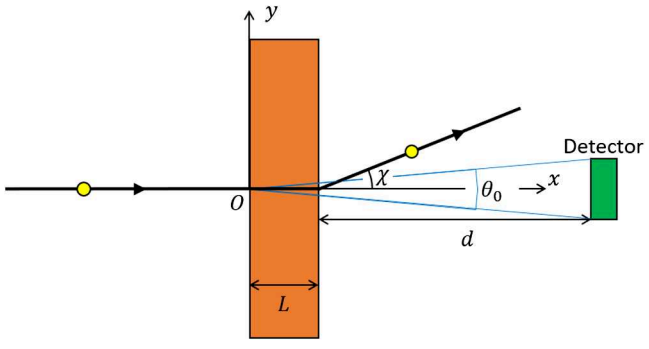

FIG. 2. Anglelike trajectory. χ is the electron deflection angle, L is the target thickness, and d is the distance between the target and the detector.

As in (6), we have neglected the quantity $-i\mu c/\omega$ in the denominators of the second terms in (9) and (10), since it is small compared to ω_p^2/ω^2 under the considered conditions.

In (8), we additionally took into account the radiation attenuation in air on its way to the detector, just multiplying $d^2N/d\omega do$ by the factor $e^{-\mu_a d}$, where $\mu_a(\omega)$ is the energy attenuation coefficient in air [43]. This was done to ensure better consistency with our subsequent analysis of radiation for realistic circular particle trajectories in a magnetic field, where attenuation in air is taken into account. It is motivated by the fact that experiments on x-ray TR by high-energy electrons, where the photon energies are typically higher than about 10 keV, can be performed in air without vacuum equipment, as reported, e.g., in [18,19].

The photon spectral density can be obtained via numerical integration of (8) over the detector acceptance region defined by the angle θ_0. For the analysis, we choose the following values of the relevant parameters: the target thickness is $L = 50$ μm, the target material is aluminum ($\omega_p = 32.86$ eV), the electron energy is $E = 4$ GeV, the distance between the target and the detector is $d = 150$ cm, and the detector acceptance angle is $\theta_0 = 2$ mrad. The calculated radiation spectral densities registered by the detector (which we further call spectra, for simplicity) for various electron deflection angles are presented in Fig. 3. The figure demonstrates a noticeable modification of the radiation spectrum, compared to that of TR for a rectilinear particle trajectory ($\chi = 0$), when the deflection angle exceeds $1/\gamma$. The pattern of this modification is rather diverse: in some regions of ω, the radiation is suppressed, while in others, it is enhanced. A more distinct picture is obtained if one considers the total number of photons N in a certain frequency interval, which are registered by the detector. For instance, Fig. 4(a) shows the dependence of this number in the range $\omega \in [5, 25]$ keV on the electron deflection angle χ. Here we see that with the increase of this

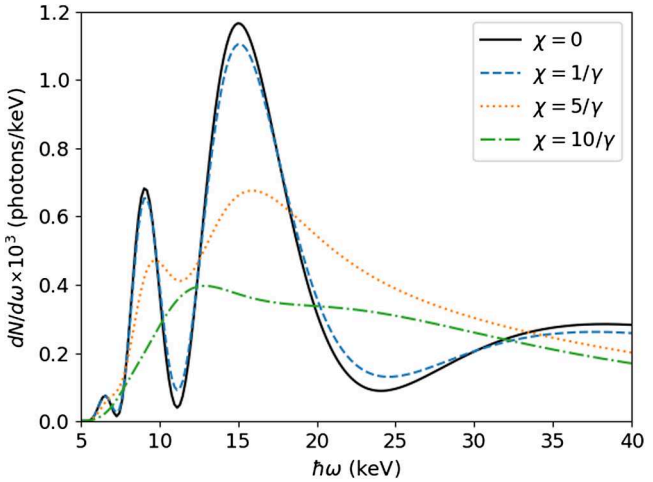

FIG. 3. Radiation spectra for the case shown in Fig. 2 for different particle deflection angles.

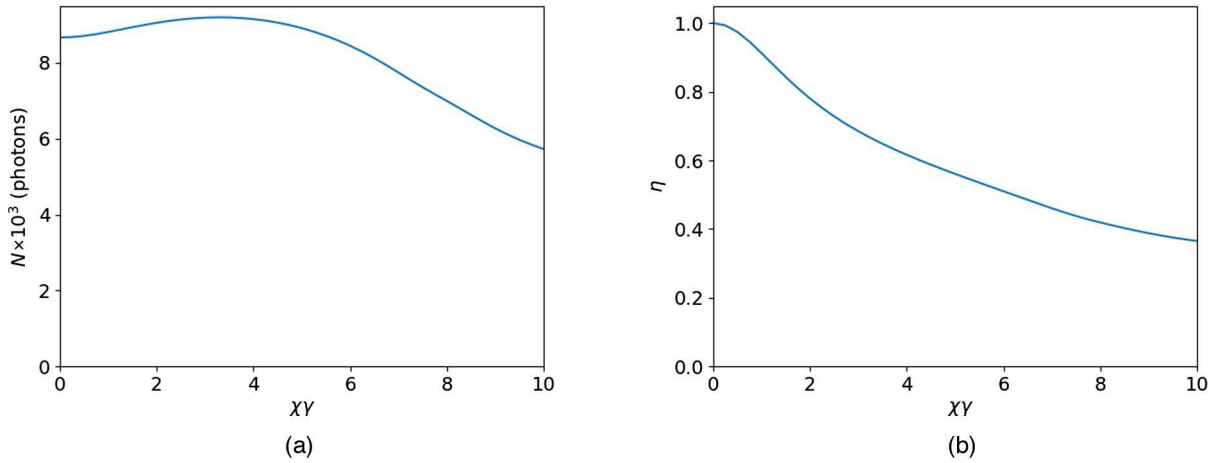

FIG. 4. Major overall characteristics of the emission for the case shown in Fig. 2. (a) Total number of photons registered by the detector and (b) ratio $\eta = N/(N_{\mathrm{TR}} + N_B)$ characterizing the interference effects.

angle the value of N first increases and then drops. The increase of N is caused by the contribution of bremsstrahlung emitted as a result of the particle deflection at the exit of the target.[3] With the further increase of χ, the intensity of this radiation increases, but its destructive interference with TR results in the decrease of the total radiation intensity.

Figure 4(a), demonstrating the total radiation intensity, however, does not provide a distinct picture of the magnitude of the discussed interference. This magnitude can be characterized by the ratio $\eta = N/(N_{\mathrm{TR}} + N_{\mathrm{B}})$, where N is the total number of emitted photons, N_{TR} is the number of pure TR photons emitted for a rectilinear particle trajectory, and N_{B} is the number of pure bremsstrahlung photons emitted for an anglelike trajectory in the absence of the target. The dependence of this ratio on χ, presented in Fig. 4(b), shows that in fact the interference between the TR and bremsstrahlung in the considered case is destructive in the whole region of the deflection angles, regardless of the fact that the total radiation is enhanced compared to the pure TR for χ less than several $1/\gamma$. The situation is analogous for other acceptance angles θ_0 and electron energies as well.

IV. CIRCULAR TRAJECTORY IN THE MAGNETIC FIELD

Let us now consider radiation of an electron which moves along a realistic circular trajectory in a magnetic field and crosses a thin target (Fig. 5). For a distance of $d = 150$ cm between the target and the detector, a detector acceptance angle of less than several mrad, and a magnetic field of 1.5 T, as we presently consider, the effective part of the electron trajectory near the target that contributes to the detected radiation amounts to several cm. In this region, we can neglect the inhomogeneities of the magnetic field, which are present in a real magnet. Moreover, the exact shape of the particle trajectory outside this effective region is not important, since radiation from that part is not detected (as assumed), allowing us to choose it in the most convenient way. For this reason, the particle trajectory is chosen to consist of three parts: straight line followed by a segment of a circle of radius R, followed again by a straight line. The particle deflection angle χ on each side of the target is chosen to exceed the half of the detector acceptance angle $\theta_0/2$ by not less than $10/\gamma$. We neglect a rather weak influence of the air on the process of radiation emission in the present case (i.e., instead of air-target boundaries, we consider vacuum-target boundaries), taking into account just the influence of the air on the radiation propagation by the factor $e^{-\mu_a d}$.

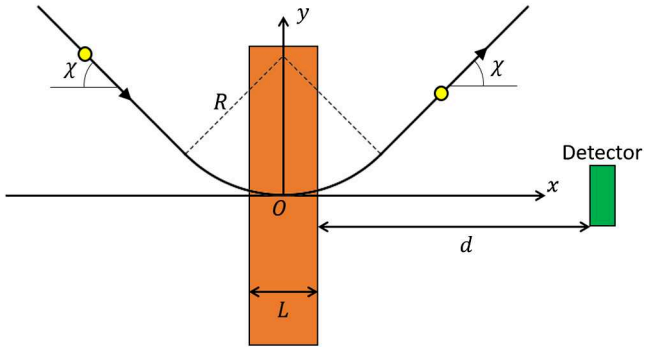

FIG. 5. Considered electron trajectory. Here χ is the deflection angle on each side of the target, L is the thickness of the target, d is the distance between the target and the detector, and R is the curvature radius of the trajectory.

[3]Let us note that by bremsstrahlung we presently mean just the radiation due to the particle deflection at the exit of the target, and we do not include here the radiation due to multiple scattering of the particle inside the target. For sufficiently thin targets considered here, this radiation can be neglected. We also neglect the impact of the particle multiple scattering in the target on its trajectory.

Applying the method described in Sec. II, one can obtain the following expression for the spectral-angular density of the number of emitted photons in this case:

$$\frac{d^2N}{dod\omega} = e^{-\mu_a d}\frac{\alpha}{4\pi^2\omega}|\mathbf{J}|^2, \tag{11}$$

where:

$$\mathbf{J} = e^{\psi}\mathbf{T}(-\chi) - \mathbf{T}(\chi) + e^{\psi}\mathbf{F}(-\chi, -L/2R) + \mathbf{F}(L/2R, \chi) + \frac{R\omega}{c}\int_{-L/2R}^{L/2R} da\mathbf{X}(a)\exp\left[\frac{i\omega R}{v}g(a) - \frac{R\psi\sin a}{L} + \frac{\psi}{2}\right] \tag{12}$$

and

$$\psi = -\mu L/2 - i\omega_p^2 L/2\omega c,$$
$$g(a) = a - \beta\sin a\cos\vartheta - \beta(1-\cos a)\sin\vartheta\cos\phi,$$
$$\mathbf{X}(a) = \mathbf{e}_y\vartheta\sin\phi + \mathbf{e}_z(a - \vartheta\cos\phi),$$
$$\mathbf{F}(a,b) = \frac{\omega R}{c}\int_a^b dx\mathbf{X}(x)\exp\left[i\omega R g(x)/v\right],$$
$$\mathbf{T}(\chi) = -2i\mathbf{X}(\chi)\exp[i\omega R g(\chi)/v]/Q(\chi).$$

Here $\beta = v/c$ is the dimensionless velocity, $\mathbf{e}_y$ and $\mathbf{e}_z$ are unit vectors along the y and z axes, and $Q(x)$ is the same function as $Q(\chi)$ in (9).

In order to obtain the number of photons registered by the detector, one has to perform numerical integration of (11) with respect to the detector acceptance region. For the analysis, we use the following values for the corresponding parameters: aluminum target thicknesses of $L = 50$ μm and $L = 12$ μm, a distance $d = 150$ cm between the target and the detector, electron energies of 2, 4, 6, and 10 GeV, the detector acceptance angles θ_0 of 2, 1, 0.4, and 0.2 mrad. All calculations were performed for a fixed magnetic field value of $B = 1.5$ T. The chosen parameters are approximately those achievable at the beamline TB21 of the DESY II test beam facility [44], where the corresponding experimental investigation is planned.[4]

Figure 6 shows the spectra for 6 GeV electron energy, 12 μm target thickness, and the total detector acceptance angle of $\theta_0 = 1$ mrad.[5] The orange dotted line shows the conventional TR spectrum for a rectilinear particle trajectory in the absence of the magnetic field. The black solid curve represents the total radiation spectrum when the target is placed in the magnetic field. The dashed blue line shows the spectrum of synchrotron radiation (SR) in the magnetic field when the target is absent. However, it is not a "pure" SR spectrum, since we additionally take into account a partial attenuation of this radiation in the target when the target is present and a part of this radiation, emitted before the particle passage through the target, penetrates through it.[6] It is this partially attenuated spectrum that should be subtracted from the total spectrum to evaluate the magnitude of the TR modification in the present case (by comparing the result with the TR spectrum for a rectilinear trajectory). The result of this subtraction is presented in Fig. 6 by the green dot-dashed line. We see that in this case it is lower than the conventional TR spectrum, which can be interpreted as the effect of TR suppression. It can be considered as a result of destructive interference of TR and SR, which results in a difference of the total radiation spectrum from the sum of independent contributions from TR (for a rectilinear trajectory) and SR.

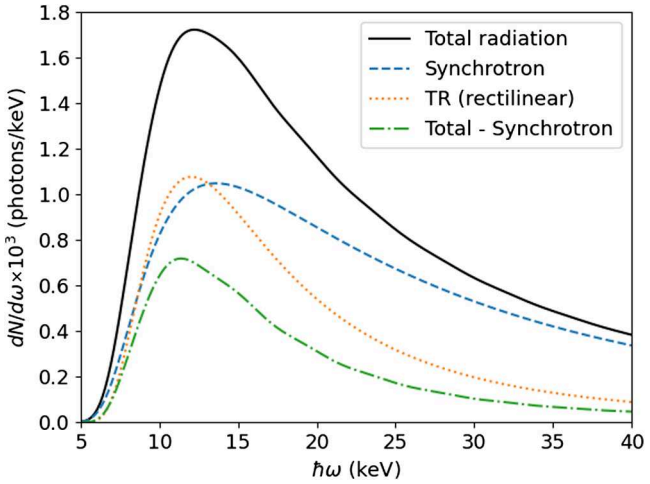

FIG. 6. Radiation spectra for the circular particle trajectory. Electron energy is 6 GeV, detector acceptance angle is 1 mrad, target thickness is 12 μm, electron deflection angle is $\chi = 22/\gamma$, and trajectory curvature radius is 13.34 m.

As Fig. 6 also shows, the intensity of SR is presently comparable to that of TR and can exceed it. Therefore, rather than focusing solely on TR, it is more consistent to investigate the interference effect as a difference between the total radiation spectrum and the sum of independent spectra of TR and SR. Figure 7 shows these spectra for the target thicknesses L of 50 μm [(a), (c), (e)] and 12 μm [(b), (d), (f)] for two values of the electron energy and the detector acceptance angle. The black solid lines demonstrate the radiation spectra from the target in the magnetic

[4]Some values, such as the 10 GeV electron energy, which lie beyond the achievable range of the mentioned facility, are considered to provide a more complete picture of the investigated effects.

[5]The positions of the maxima of the presented spectra and, in some cases, the existence of these maxima themselves, are mostly defined by radiation attenuation in air.

[6]Neglecting the part of SR emitted inside the target, this spectrum can be presented as a sum of the half of the pure SR spectrum, created after the particle passage of the target, and the half of the spectrum, created before it, multiplied by the factor $e^{-\mu L}$.

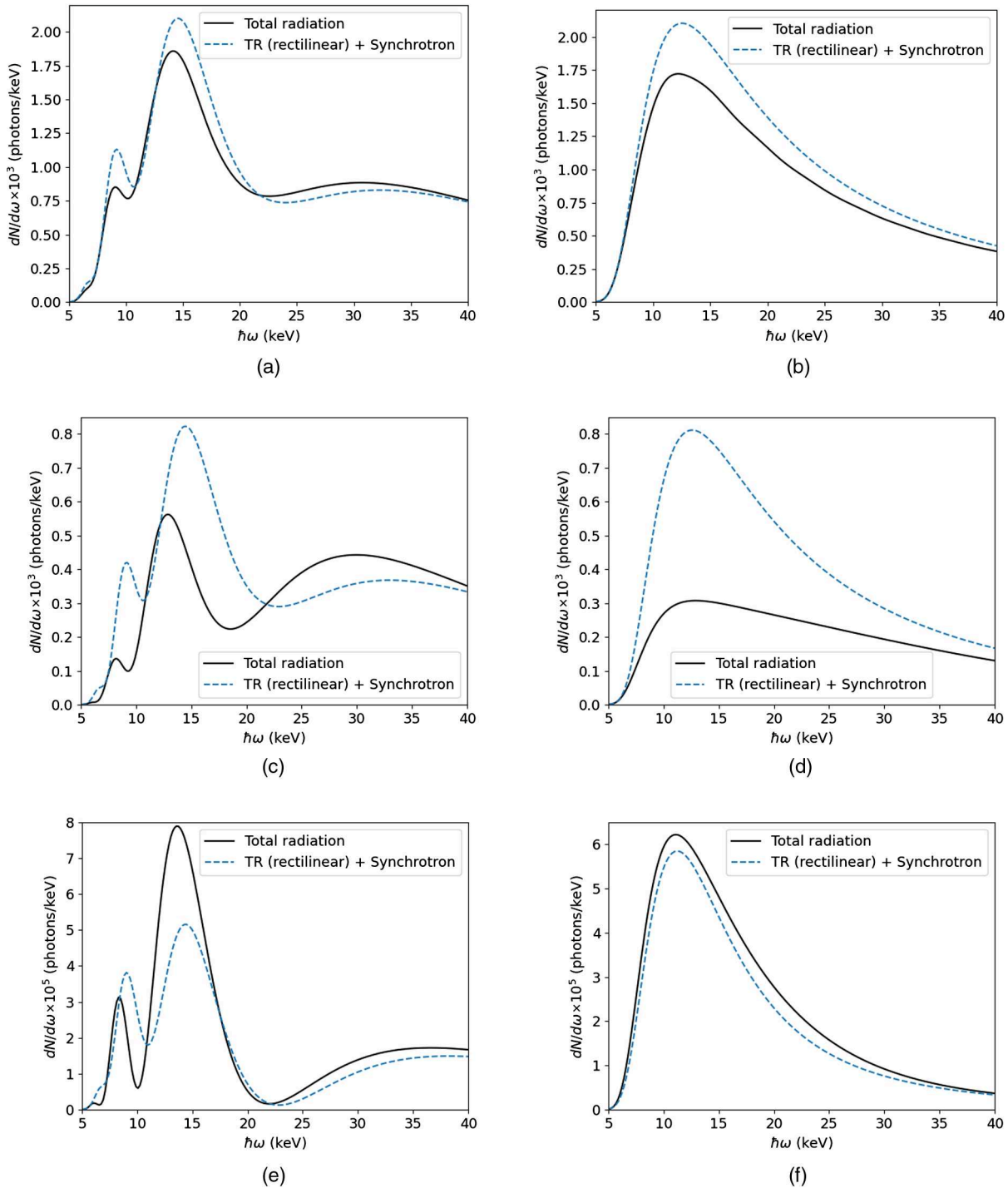

FIG. 7. Total radiation spectrum and the sum of independent spectra of TR (for a rectilinear trajectory) and SR for different target thicknesses, electron energies, and detector acceptance angles: (a) 6 GeV, 1 mrad, 50 μm; (b) 6 GeV, 1 mrad, 12 μm; (c) 6 GeV, 0.4 mrad, 50 μm; (d) 6 GeV, 0.4 mrad, 12 μm; (e) 2 GeV, 0.4 mrad, 50 μm; and (f) 2 GeV, 0.4 mrad, 12 μm.

field, the dashed blue lines show the sum of independent spectra of TR (for a rectilinear trajectory) and SR (taking into account its attenuation in the target). The shapes of the spectra for different L differ from each other due to various values of the factor which describes the interference of the TR waves emitted at the upstream and the downstream surfaces of the target. In particular, for $L = 50$ μm, this interference leads to the appearance of oscillations in the low-frequency part of the spectrum, which are not completely damped by attenuation in the air.

In Fig. 7, we see that for the electron energy of $E = 6$ GeV the radiation is mostly suppressed and the interference is

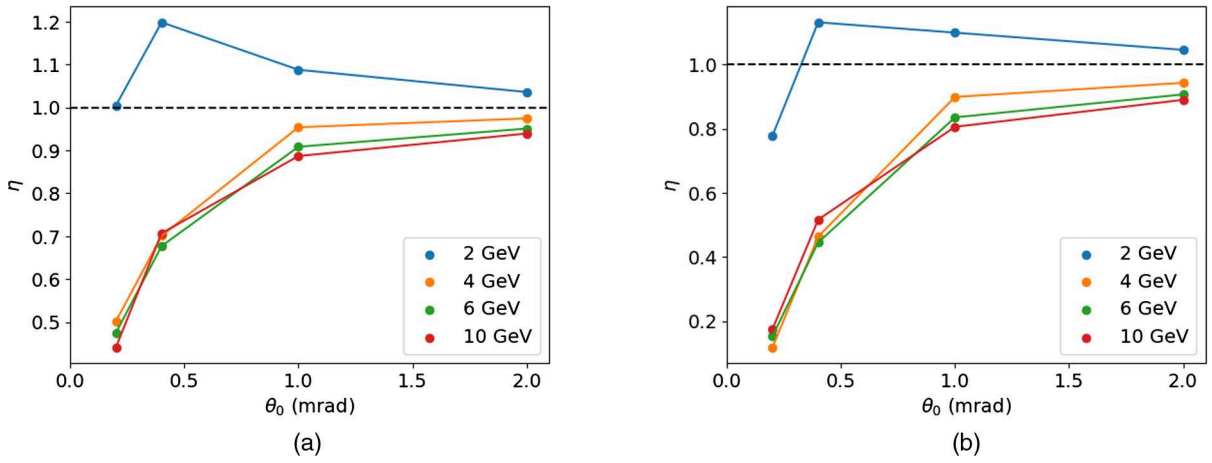

FIG. 8. Dependence of the ratio $\eta = N/(N_{\mathrm{TR}} + N_{\mathrm{SR}})$ on the acceptance angle θ_0. (a) Target thickness is 50 μm and (b) target thickness is 12 μm.

destructive, except for the high-frequency region in the case of the 50 μm target. The interference effects noticeably increase with the decrease of the detector acceptance angle. Particularly, for $L = 12$ μm and $\theta_0 = 0.4$ mrad, we observe a huge radiation suppression in the region around the maximum of the spectrum. The situation is completely different for $E = 2$ GeV. In this case, for $L = 12$ μm a weak constructive interference occurs in the whole presented range of frequencies. For $L = 50$ μm a strong constructive interference is observed in the region of the main maximum.

In order to see a more distinct overall picture of the interference effects in the present case, let us consider the total number of photons emitted in the frequency region of $\omega \in [5, 25]$ keV, as in Sec. III. Figure 8 shows the dependence of the ratio $\eta = N/(N_{\mathrm{TR}} + N_{\mathrm{SR}})$ on the detector acceptance angle for two values of the target thickness and various electron energies shown in the legend. Currently, N is the number of photons in the total radiation spectrum; N_{TR} is the number of photons in the TR spectrum for a rectilinear particle trajectory; and N_{SR} is the number of SR photons. The ratio η was calculated for the values $\theta_0 = 0.2, 0.4, 1$, and 2 mrad, and the corresponding points in the figures are connected by straight lines for convenience.

Figures 8(a) and 8(b) show that for energy of 4 GeV and higher, the interference between TR and SR is destructive for all acceptance angles in the presented region. For relatively large values of θ_0, the destructive interference becomes slightly more pronounced as the electron energy increases. For the mentioned energies (4 GeV and above), the destructive interference becomes stronger with the decrease of the acceptance angle, and for sufficiently small θ_0 the radiation can be dramatically suppressed compared to the sum of independent TR and SR. Comparing Figs. 8(a) and 8(b), we see that for the target of thickness 12 μm, this suppression is stronger than for 50 μm. This may be associated with the fact that for $L = 12$ μm the spectra do not have oscillations and the radiation suppression occurs for all frequencies, while for $L = 50$ μm, due to oscillations, the regions of the destructive interference alternate with the regions where the interference is constructive. The situation is different for lower electron energies. In particular, for $E = 2$ GeV, the constructive interference can take place for the frequency-integrated number of photons. In this case, the dependence of η on θ_0 can reach a maximum at some value of the acceptance angle.

The qualitative behavior of η as a function of E and θ_0 can be understood from considerations involving the radiation formation length l_F (at least in the region of the destructive interference where $\eta < 1$). Generally, it can be expected that TR, and the total radiation as well (when compared to the sum of TR and SR), should be suppressed if the particle deflection angle within l_F exceeds $1/\gamma$, since in this case the particle leaves the typical radiation cone before TR is properly formed. This expectation is supported by Fig. 4(b) for a simpler case of an anglelike particle trajectory, where the deflection to the angle χ occurs within the formation length for any frequency. Figure 9 shows the dependence of the particle deflection angle l_F/R within the formation length (7) on the observation angle ϑ, in units of $1/\gamma$. This dependence is generated by the decrease of l_F with increasing ϑ. The formation length is calculated in vacuum ($\omega_p = 0$), for the frequency of $\omega = 14$ keV approximately corresponding to the position of the main maximum of the spectra in Fig. 7. The region of ϑ in Fig. 9 (up to 1 mrad) corresponds to the largest detector acceptance angle of 2 mrad presented in Fig. 8. The values of ϑ, corresponding to other acceptance angles (via $\vartheta = \theta_0/2$) for which the ratio η was calculated, are marked by vertical lines.

In Fig. 9, we see that for electron energies of 4 GeV and higher, the deflection angle within l_F is larger than 1 (in units of $1/\gamma$) at sufficiently small ϑ and manifestation of the destructive interference could be expected. However, according to Fig. 8, it is rather small for relatively large acceptance angles of about 2 mrad. Figure 9 indicates that it

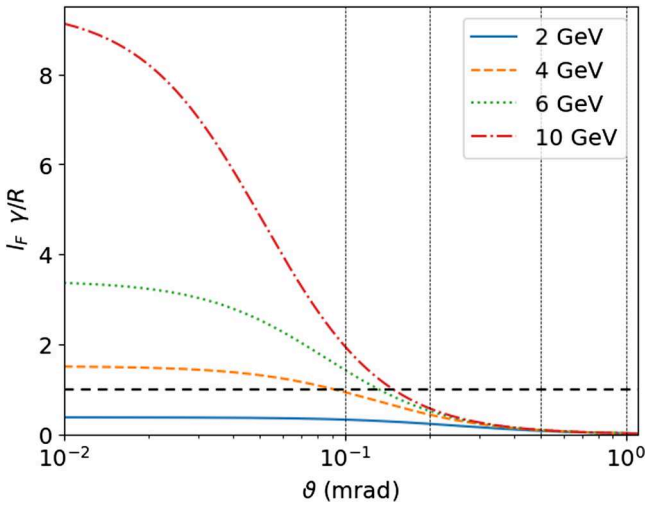

FIG. 9. Dependence of the deflection angle (in units of $1/\gamma$) within the formation length on the observation angle ϑ for the frequency $\omega = 14$ keV and different electron energies. The horizontal dashed line marks the value $l_F\gamma/R = 1$. The vertical lines mark the angles corresponding to the detector acceptance angles in Fig. 8 as $\vartheta = \theta_0/2$.

is caused by the fact that in the major part of the region of ϑ, contributing to the detected radiation in these cases, the deflection angle is smaller (or much smaller) than 1. The region where the deflection angle exceeds 1, slightly grows with the increase of E. Together with the increase of the values of the deflection angle in this region, this leads to a slight increase in the magnitude of the destructive interference. The interference is stronger for smaller values of θ_0, since in this case the deflection angle exceeds 1 in a larger part of the region of ϑ, contributing to the detected radiation.

V. CONCLUSIONS

In the present work, we investigated the influence of a strong magnetic field on x-ray radiation emitted when a high-energy electron passes through a thin foil placed in this field. In the absence of the field, this radiation is conventional x-ray transition radiation (TR). In the presence of the field, synchrotron radiation (SR) is generated as well. The parameters are chosen to approximately correspond to the ones which could be achieved at the beamline TB21 of the DESY II test beam facility (the electron energies are considered in a bit wider region). It is shown that in this case the total radiation can noticeably differ from the sum of independent TR for a rectilinear particle trajectory and SR, and a strong interference between these types of emission can occur. Formally, it can be considered as a modification of TR by the bending of the particle trajectory. Such interference can be both constructive (for lower electron energies) and destructive (for higher energies). The magnitude of the constructive interference changes nonmonotonously with the change of the detector acceptance angle, while the magnitude of the destructive interference increases with the decrease of this angle. This magnitude also grows with the increase of the particle energy. The physical reasons for this are discussed involving the concept of the radiation formation length.

ACKNOWLEDGMENTS

The work of S. V. T. and G. K. was partially supported by the Project No. 531314364 of the German Research Foundation (STCU Project No. P811). The work of S. V. T. was also partially supported by the Project No. 0124U002155 of the National Academy of Sciences of Ukraine. The work of A. V. S. was partially supported through the MSCA4Ukraine Project No. 1233244, which is funded by the European Union.

DATA AVAILABILITY

The data that support the findings of this article are not publicly available upon publication because it is not technically feasible and/or the cost of preparing, depositing, and hosting the data would be prohibitive within the terms of this research project. The data are available from the authors upon reasonable request.

[1] L. Wartski, S. Roland, J. Lasalle, M. Bolore, and G. Filippi, Interference phenomenon in optical transition radiation and its application to particle beam diagnostics and multiple scattering measurements, J. Appl. Phys. **46**, 3644 (1975).
[2] R. B. Fiorito and D. W. Rule, Optical transition radiation beam emittance diagnostics, AIP Conf. Proc. **319**, 21 (1994).
[3] H.-C. Lihn, P. Kung, C. Settakorn, H. Wiedemann, and D. Bocek, Measurement of subpicosecond electron pulses, Phys. Rev. E **53**, 6413 (1996).
[4] B. Dolgoshein, Transition radiation detectors, Nucl. Instrum. Methods Phys. Res., Sect. A **326**, 434 (1993).
[5] P. Rullhusen, X. Artru, and P. Dhez, *Novel Radiation Sources Using Relativistic Electrons: From Infrared to X-Rays* (World Scientific, Singapore, 1998).
[6] V. N. Baier and V. M. Katkov, Transition radiation as a source of quasi-monochromatic x-rays, Nucl. Instrum. Methods Phys. Res., Sect. A **439**, 189 (2000).
[7] O. Kettig, H. Backe, N. Clawiter *et al.*, A novel type of x-ray interferometer, AIP Conf. Proc. **506**, 669 (2000).
[8] F. Hagenbuck, H. Backe, N. Clawiter *et al.*, Novel digital K-edge imaging system with transition radiation from an 855-MeV electron beam, IEEE Trans. Nucl. Sci. **48**, 843 (2001).
[9] V. L. Ginzburg and V. N. Tsytovich, *Transition Radiation and Transition Scattering* (Adam Hilger, Bristol, 1984).
[10] E. L. Feinberg, High energy successive interactions, Sov. Phys. JETP **23**, 132 (1966), http://jetp.ras.ru/cgi-bin/e/index/e/23/1/p132?a=list.
[11] N. F. Shul'ga, S. V. Trofymenko, and V. V. Syshchenko, On the transition radiation and bremsstrahlung from a relativistic electron with a nonequilibrium field, JETP Lett. **93**, 1 (2011).

[12] Y. Shibata, K. Ishi, T. Takahashi, T. Kanai, F. Arai, S.-I. Kimura, T. Ohsaka, M. Ikezawa, Y. Kondo, R. Kato, S. Urasawa, T. Nakazato, S. Niwano, M. Yoshioka, and M. Oyamada, Coherent transition radiation in the far-infrared zone, Phys. Rev. E **49**, 785 (1994).

[13] S. V. Trofymenko, N. F. Shul'ga, N. Delerue, S. Jenzer, V. Khodnevych, and A. Migayron, Proposal to observe half-bare electrons on 45-MeV linac, J. Phys. Conf. Ser. **874**, 012076 (2017).

[14] R. Kieffer, M. Bergamaschi, E. Bravin, W. Farabolini, P. Karataev, T. Lefevre, and S. Mazzoni, Experimental observation of "shadowing" in optical transition radiation, Phys. Rev. Lett. **120**, 094802 (2018).

[15] A. Curcio, M. Bergamaschi, R. Corsini, D. Gamba, W. Farabolini, R. Kieffer, T. Lefevre, S. Mazzoni, V. Dolci, M. Petrarca, P. Karataev, K. Lekomtsev, S. Lupi, and A. Potylitsyn, Diffractive shadowing of coherent polarization radiation, Phys. Lett. A **391**, 127135 (2021).

[16] M. L. Cherry, G. Hartmann, D. Müller, T. A. Prince, M. L. Cherry, G. Hartmann, D. Müller, and T. A. Prince, Transition radiation from relativistic electrons in periodic radiators, Phys. Rev. D **10**, 3594 (1974).

[17] H. Backe, S. Gampert, A. Grendel, H.-J. Hartmann, W. Lauth, C. Weinheimer, R. Zahn, F. R. Buskirk, H. Euteneuer, K. H. Kaiser, G. Stephan, and T. Walcher, Resonant transition radiation in the x-ray region from a low emittance 855 MeV electron beam, Z. Phys. A **349**, 87 (1994).

[18] S. V. Trofymenko, R. M. Nazhmudinov, A. V. Shchagin, A. S. Kubankin, A. P. Potylitsyn, A. S. Gogolev, N. A. Filatov, G. Kube, N. A. Potylitsina-Kube, M. Stanitzki, R. Diener, and A. Novokshonov, Formation region effects in x-ray transition radiation from 1 to 6 GeV electrons in multilayer targets, Nucl. Instrum. Methods Phys. Res., Sect. B **476**, 44 (2020).

[19] V. R. Kocharyan, G. Kube, S. Strokov *et al.*, Observation of x-ray transition radiation from a relativistic electron passing a stack of plates, Nucl. Instrum. Methods Phys. Res., Sect. A **1075**, 170418 (2025).

[20] L. D. Landau and I. Y. Pomeranchuk, The limits of applicability of the theory of bremsstrahlung by electrons and of the creation of pairs at large energies, Dokl. Akad. Nauk SSSR **92**, 535 (1953); *Collected Papers of L. D. Landau*, edited by D. ter Haar (Pergamon Press, Oxford, 1965), pp. 586–588.

[21] A. B. Migdal, Bremsstrahlung and pair production in condensed media at high energies, Phys. Rev **103**, 1811 (1956).

[22] P. L. Anthony, R. Becker-Szendy, P. E. Bosted, M. Cavalli-Sforza, L. P. Keller, L. A. Kelley, S. R. Klein, G. Niemi, M. L. Perl, L. S. Rochester, and J. L. White, An accurate measurement of the Landau-Pomeranchuk-Migdal effect, Phys. Rev. Lett. **75**, 1949 (1995).

[23] F. F. Ternovskii, On the theory of radiative processes in piecewise homogeneous media, Sov. Phys. JETP **12**, 123 (1961), http://jetp.ras.ru/cgi-bin/e/index/e/12/1/p123?a=list.

[24] N. F. Shul'ga and S. P. Fomin, Suppression of radiation in an amorphous medium and in a crystal, JETP Lett. **27**, 117 (1978), http://jetpletters.ru/ps/1545/article_23655.shtml.

[25] H. D. Thomsen, J. Esberg, K. Kirsebom, H. Knudsen, E. Uggerhøj, U. I. Uggerhøj, P. Sona, A. Mangiarotti, T. J. Ketel, A. Dizdar, M. M. Dalton, S. Ballestrero, and S. H. Connell, On the macroscopic formation length for GeV photons, Phys. Lett. B **672**, 323 (2009).

[26] M. L. Ter-Mikaelyan, Bremsstrahlung radiation spectrum in a medium, Dokl. Akad. Nauk SSSR **94**, 1033 (1954).

[27] G. Naumenko, X. Artru, A. Potylitsyn, Y. Popov, L. Sukhikh, and M. Shevelev, "Shadowing" of the electromagnetic field of relativistic charged particles, J. Phys. Conf. Ser. **236**, 012004 (2010).

[28] S. V. Trofymenko, X-ray emission by a high-energy electron with a nonequilibrium field in an ultrathin crystal, Phys. Rev. A **98**, 023813 (2018).

[29] S. V. Trofymenko, N. F. Shul'ga, and A. V. Shchagin, Diffracted x-ray transition radiation by a "half-bare" electron, Phys. Rev. Accel. Beams **22**, 024501 (2019).

[30] N. F. Shul'ga and S. V. Trofymenko, On ionization energy losses of ultra-relativistic half-bare electron, Phys. Lett. A **376**, 3572 (2012).

[31] R. A. Bosch, Extraction of edge radiation within a straight section of Aladdin, Rev. Sci. Instrum. **73**, 1423 (2002).

[32] G. D. Fleishman, Suppression of transition radiation by a magnetic field, Sov. Phys. JETP **72**, 272 (1991), http://jetp.ras.ru/cgi-bin/e/index/e/72/2/p272?a=list.

[33] M. I. Ryazanov, Angular distribution of transient radiation from an ultrarelativistic particle in a magnetic field, J. Exp. Theor. Phys. **98**, 478 (2004).

[34] M. Brigida, C. Favuzzi, P. Fusco, F. Gargano, N. Giglietto, F. Giordano, F. Loparco, B. Marangelli, M. N. Mazziotta, N. Mirizzi, S. Rainò, and P. Spinelli, The silicon transition radiation detector: Performance and perspectives, Nucl. Instrum. Methods Phys. Res., Sect. A **572**, 440 (2007).

[35] ALICE Collaboration, The ALICE transition radiation detector: Construction, operation, and performance, Nucl. Instrum. Methods Phys. Res., Sect. A **881**, 88 (2018).

[36] G. M. Garibyan, Radiation of a particle moving across the interface of two media with account of multiple scattering, Sov. Phys. JETP **12**, 237 (1961), http://jetp.ras.ru/cgi-bin/e/index/e/12/2/p237?a=list.

[37] G. M. Garibyan and Yan Shi, X-ray emission by an ultrarelativistic charge in a plate with allowance for multiple scattering, Sov. Phys. JETP **43**, 848 (1976), http://jetp.ras.ru/cgi-bin/e/index/e/43/5/p848?a=list.

[38] L. D. Landau and E. M. Lifshitz, *The Classical Theory of Fields* (Pergamon, Oxford, 1971).

[39] https://henke.lbl.gov/optical_constants/atten2.html.

[40] J. D. Jackson, *Classical Electrodynamics* (Wiley, New York, 1962).

[41] L. Durand, Transition radiation from ultrarelativistic particles, Phys. Rev. D **11**, 89 (1975).

[42] A. P. Potylitsyn, *Electromagnetic Radiation of Electrons in Periodic Structures* (Springer, Berlin, 2011).

[43] https://physics.nist.gov/PhysRefData/XrayMassCoef/tab4.html.

[44] R. Diener, J. Dreyling-Eschweiler, H. Ehrlichmann, I. M. Gregor, U. Kötz, U. Krämer, N. Meyners, N. Potylitsina-Kube, A. Schütz, P. Schütze, and M. Stanitzki, The DESY II test beam facility, Nucl. Instrum. Methods Phys. Res., Sect. A **922**, 265 (2019).